AIP | Review of Scientific Instruments

A trap-based pulsed positron beam optimised for positronium laser spectroscopy

B. S. Cooper, A. M. Alonso, A. Deller, T. E. Wall, and D. B. Cassidy

Citation: Review of Scientific Instruments **86**, 103101 (2015); doi: 10.1063/1.4931690
View online: http://dx.doi.org/10.1063/1.4931690
View Table of Contents: http://scitation.aip.org/content/aip/journal/rsi/86/10?ver=pdfcov
Published by the AIP Publishing

A trap-based pulsed positron beam optimised for positronium laser spectroscopy

B. S. Cooper,[a] A. M. Alonso, A. Deller, T. E. Wall, and D. B. Cassidy
Department of Physics and Astronomy, University College London, Gower Street, London WC1E 6BT, United Kingdom

(Received 1 July 2015; accepted 13 September 2015; published online 1 October 2015)

We describe a pulsed positron beam that is optimised for positronium (Ps) laser-spectroscopy experiments. The system is based on a two-stage Surko-type buffer gas trap that produces 4 ns wide pulses containing up to 5×10^5 positrons at a rate of 0.5-10 Hz. By implanting positrons from the trap into a suitable target material, a dilute positronium gas with an initial density of the order of 10^7 cm^{-3} is created in vacuum. This is then probed with pulsed (ns) laser systems, where various Ps-laser interactions have been observed via changes in Ps annihilation rates using a fast gamma ray detector. We demonstrate the capabilities of the apparatus and detection methodology via the observation of Rydberg positronium atoms with principal quantum numbers ranging from 11 to 22 and the Stark broadening of the $n = 2 \rightarrow 11$ transition in electric fields. © *2015 AIP Publishing LLC.* [http://dx.doi.org/10.1063/1.4931690]

I. INTRODUCTION

Low-energy mono-energetic positron beams derived from a radioactive isotope (RI) were first developed in the early 1970s,[1] and since that time they have been improved such that they can now provide beam strengths of up to 10^7 positrons/s. This is sufficient to perform a wide variety of experimental studies of positron and positronium (Ps) physics,[2,3] but is less than ideal for studies of positronium-light interactions, which generally require higher beam strengths. As a result, optical spectroscopy of Ps has historically been quite limited. Some experiments[4–6] were successfully carried out in the 1980s and 1990s using a magnetic bottle trap[7] or intrinsically pulsed accelerator-based positron beams,[8,9] which can provide high instantaneous positron intensities. Recently, photodetachment of Ps negative ions has been performed using the pulsed output from a LINAC based positron beam.[10,11] However, the availability of such beams was and is limited, and experimentation in this area correspondingly sparse.

The development of the Surko buffer gas positron trap[12,13] has now made it considerably easier to obtain larger numbers of positrons in pulses using a standard RI based beam. This device captures and cools positrons from a DC source in a Penning trap via interactions with gas molecules. The stored positrons may be used in different ways; by slowly releasing thermalised particles, one may produce a high-quality DC beam with a very low energy spread ($\Delta E \sim 25$ meV),[14] which has proved to be useful in high resolution scattering experiments.[15–17] Alternatively, the stored positrons may be ejected all at once in a time-bunched pulse,[18] in which case they will have a relatively large energy spread. Pulsing the beam may be done at high repetition rates in order to perform timing measurements using individual positron events[19] or all of the stored positrons may be dumped in a single intense pulse.[4,20,21] The latter technique makes it possible to generate a dilute Ps gas and hence to study Ps-Ps interactions[22] or perform optical measurements.[7,23] There are several buffer gas positron traps in operation around the world, configured for a wide variety of different experimental goals.[19,21,24–30] Here, we describe an apparatus that is optimised for laser spectroscopy of low-density non-interacting Ps atoms.

II. APPARATUS

A. Positron beam and trap

The positron beam-line is composed of three sections, the moderated DC positron beam, the buffer-gas positron trap, and the Ps production and laser interaction region. These are depicted schematically in Figure 1.

The generation of a mono-energetic positron beam from a RI is achieved using a process known as moderation.[1,31] This involves some fraction of the fast β^+ particles entering a solid material (the moderator), losing most of their kinetic energy, and then being emitted from the moderator and transported using electromagnetic fields. The wide β^+ energy spectrum[32] is moderated to an energy spread of around 2 eV. There are many materials that can be used as moderators;[32] the most efficient currently known is solid neon,[33] which can achieve an overall efficiency of the order of 1% when the RI used is ^{22}Na. The system we describe here contains a DC positron beam derived from a 1 GBq ^{22}Na source mounted behind a conical aperture[34] that is thermally coupled to, but electrically isolated from, a 5 K closed cycle helium cryostat. The moderator is grown by admitting neon gas directly in front of the cone via a thin tube for around 8-10 min; the pressure measured in the source chamber is $\sim 1 \times 10^{-3}$ mbar during the moderator growth, although it will be higher in the region where the gas is injected. An example of a typical moderator growth sequence is shown in Figure 2(a) and its decay over time in 2(b).

A new moderator typically produces a DC beam of $\sim 6 \times 10^6$ e$^+$ s^{-1} which indicates a moderator efficiency of ~0.7%. The efficiency is defined as the ratio of the number of positrons in the beam to the source activity. This includes the 90%

[a]Electronic mail: ben.cooper.13@ucl.ac.uk

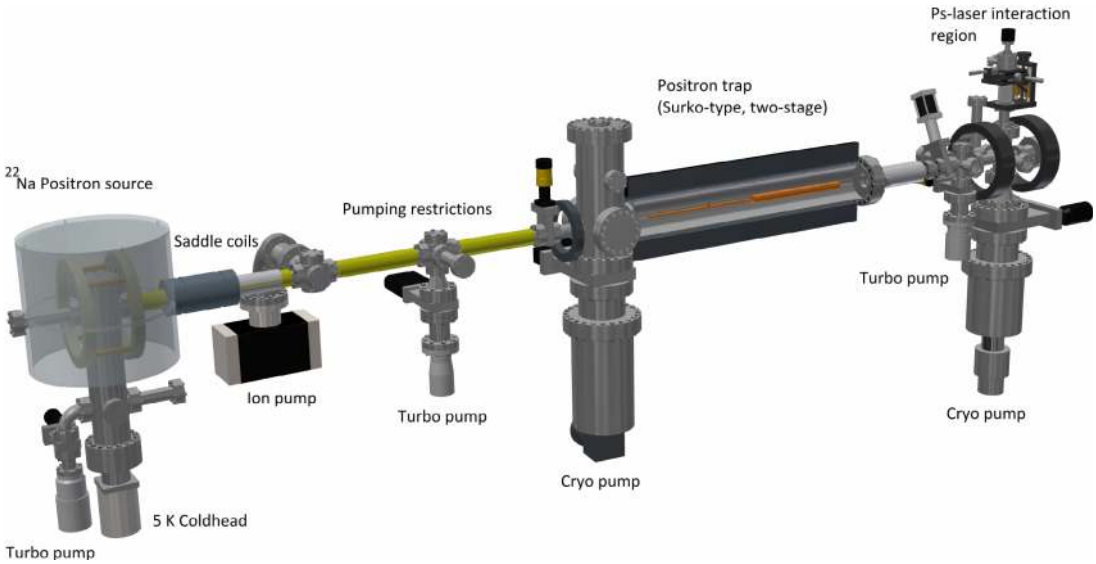

FIG. 1. Layout of the apparatus. A moderated positron beam is magnetically guided towards a two-stage Surko-type buffer gas trap which generates pulses containing up to 5×10^5 positrons and ejects them as a bunched packet ($\Delta t \sim 4$ ns) at a repetition frequency of 1 Hz. The positrons are guided towards an interaction region where positronium is created, which may then be probed with pulsed lasers. The magnetic fields at the source, in the trap center, and at the MCP detector are approximately 13, 50, and 13 mT, respectively.

branching ratio for positron emission in ^{22}Na decay, but does not consider effects due to absorption in the source material. The beam is monitored by a NaI scintillator attached to a photomultiplier tube (PMT). This is done by counting positron annihilation events that occur at the gate valve just before the entrance of the trap. The beam decays to around 50% of initial strength over the following 10-14 days. Two 15 cm long and 8 mm diameter pumping restrictions between the buffer gas trap and the source chamber limit the conductance between the two regions. The observed moderator decay is due to the vacuum conditions in the source chamber.

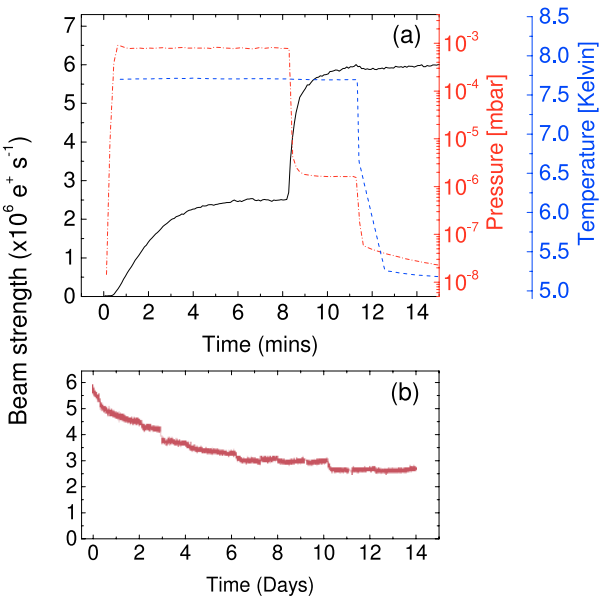

FIG. 2. (a) A typical moderator growth sequence showing a steady increase in count rate (solid line) when the neon is introduced at a constant pressure (dots and dashes). The gas inlet is closed when the count rate levels off, causing a drop in the pressure and a corresponding increase in the count rate. The temperature (dashed line) is held above the cold head base temperature (5 K) during the growth to anneal the neon deposit. (b) Decay of the beam strength following the growth sequence in (a).

Unmoderated positrons are blocked at a solid barrier, over which the slow positron beam is steered magnetically using a pair of saddle coils. The moderated beam is then guided to a two-stage Surko-type buffer-gas trap.[12,13] The system we describe is slightly different from the original Surko design as there is no accumulation stage. This two-stage version, formerly available commercially from First Point Scientific, Inc.,[20] is designed to capture a DC beam and emits positrons at a relatively fast repetition rate (from KHz to Hz), which is well suited to Ps laser spectroscopy. Our system typically operates at 1 Hz with a N_2 and a CF_4 mixture for positron capture and cooling.[35,36] Positrons lose energy through inelastic collisions with N_2 molecules in the trap. This causes axial confinement within the static potential structure applied to the trap electrodes. The potential structure and approximate pressures in the system are shown in Figure 3. Radial confinement is induced by the approximately flat magnetic field produced by the large solenoid surrounding the trap. The device differs from the standard Surko arrangement[35] insofar as it has a smaller pressure differential in the final stage and hence a relatively short positron lifetime. Radial compression of the trapped positrons is achieved with a rotating wall (RW) quadrupole electric field, operating in a non-plasma regime.[21,37,38] The RW field induces inward radial transport of the positrons, which reduces collisions with the chamber walls. This increases the lifetime of the stored positrons which is then determined only by annihilation with the buffer and cooling gases. The positron beam spot size is also reduced via this process, which is in effect a form of loss-free re-moderation[39] (i.e., phase space compression).

The Ps-laser interaction region is approximately 1 m from the trap (see Figure 1) and contains a micro-channel plate (MCP) and phosphor screen assembly which are viewed with a CCD camera. These are used to align the positrons to a

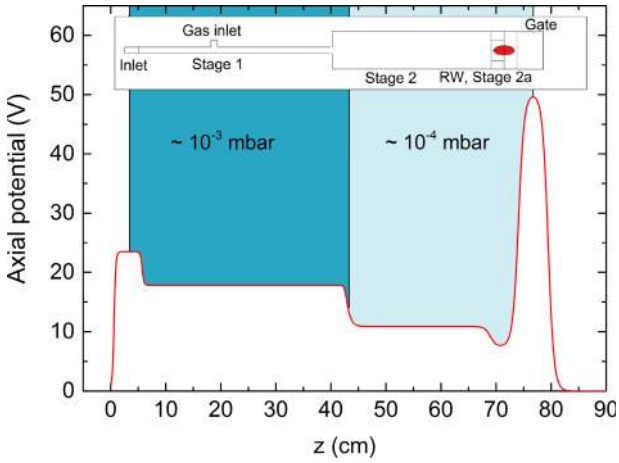

FIG. 3. The axial electric potential in the trap during the loading phase. The reduction in gas pressure from stage one to two increases the lifetime against annihilation in the second stage. The lifetime is increased further with the application of rotating wall compression.

well-defined spatial location which is then overlapped by the lasers. Images of the DC beam and the pulsed trap output are shown in Figure 4. The annular profile of the DC beam is due to the conical nature of the moderator. The design of the source[20] is such that the RI capsule is not thermally connected to the moderator cone and therefore does not get cold enough for neon gas to freeze onto its window.

The increase in the positron lifetime when the RW field is applied can be seen in Figure 5, which shows the annihilation signal of the trap output pulse as a function of fill time. The signal is proportional to the number of positrons in the pulse. These data are fitted with

$$N_{e^+}(t) = A(1 - e^{-t/\tau}), \tag{1}$$

where τ is the positron lifetime in the second stage of the trap, $A = R\tau$, and R is the positron capture rate.

The lifetime in the trap is measured as 1.72 ± 0.07 s and 0.13 ± 0.09 s with the rotating wall on and off, respectively. When the RW field is applied, the measured lifetime is almost entirely due to interactions with gas molecules. Without the RW field, positron diffusion to the electrodes leads to an increased annihilation rate.[40] The lifetime in the trap is an important factor in determining the repetition rate at which the system is most efficient. This is also informed by other factors; in the case of spectroscopy with pulsed lasers, for example, it is necessary to match the trap and laser repetition rates. A typical Nd:YAG laser operates at 10 or 20 Hz, and so for laser spectroscopy using this type of system, it would not be useful to run much faster than this, although lower frequencies can be used.[41] We find that the practical operational range for our system is roughly 0.5-10 Hz. The limit of 10 Hz is set by the repetition rate of the lasers. Figure 5 shows that the number of trapped positrons begins to saturate above a 2 s fill time, and this sets the lower limit for the trap cycle rate of 0.5 Hz.

Similar work has been performed[41] using a system designed to generate high density positron plasmas,[21] for the study of Ps-Ps interactions[42] and Ps_2 formation.[43] This device included a decoupled UHV accumulation stage and operated at a frequency of around 0.03 Hz. The apparatus we describe here is considerably less complicated. It cannot produce high positron densities, but is suitable for performing optical measurements using a low-density Ps ensemble.

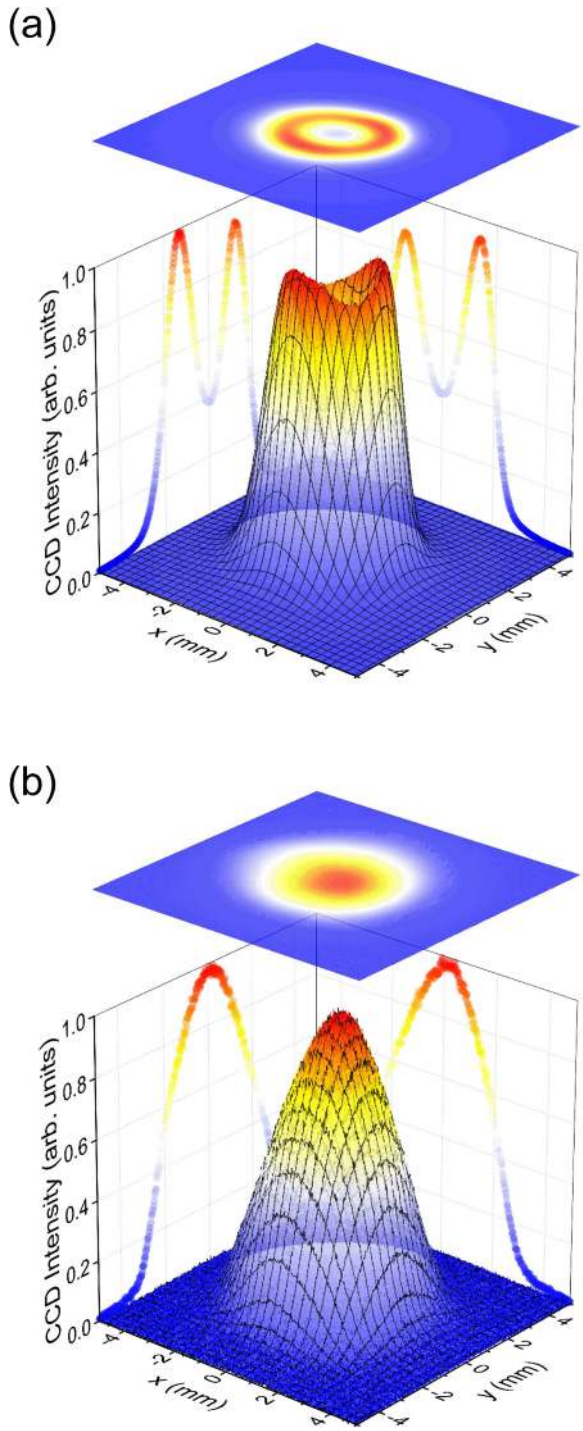

FIG. 4. (a) DC beam imaged on multichannel plate, phosphor screen assembly with a three dimensional representation and orthogonal line profiles projected onto the axes. The hole in the middle of the beam is due to the conical moderator substrate geometry. (b) Trap output pulse imaged on the same detector. Fitting of the line profiles gives a spatial pulse width of 3.33 ± 0.01 mm FWHM in the wider direction (x-axis). The observed beam size depends on the magnetic field in the target region (~13 mT). Both (a) and (b) have been normalised to the peak amplitudes. Calibration of the size of the image is performed with a 2 mm diameter alignment hole, situated at the bottom of the target holder.

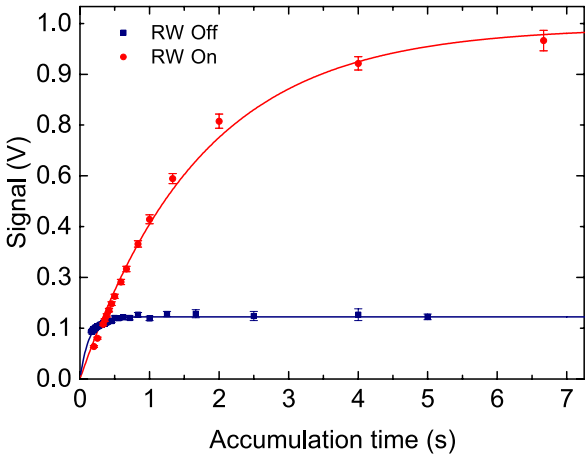

FIG. 5. Annihilation gamma ray signal of measured from the trap output as a function of positron accumulation time. The lifetime against annihilation within the trap (τ) is estimated by fitting equation (1) to the measured data and has a value of 1.72 ± 0.07 s when the rotating wall is being driven at 4 MHz and 4 V (pk-pk). The lifetime reduces to 0.13 ± 0.09 s in the absence of a rotating electric field.

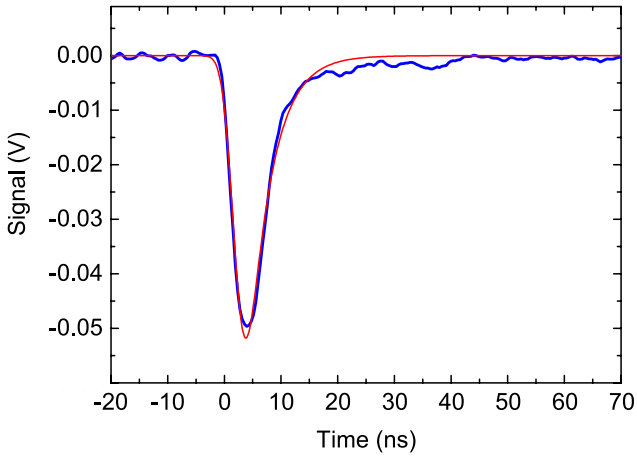

FIG. 7. Annihilation signal of 1 keV bunched positrons impacting a metal surface at 1 keV. The measurement was performed at the position of Ps production using a Cherenkov radiator and PMT. Equation (2) is fitted to the data. The width of the Gaussian gamma ray burst found from deconvolution of Eq. (2) is 3.9 ± 0.1 ns.

B. Bunched positron pulses

A key feature of the system we describe here is the ability to generate a pulsed, many-positron bunch that is well matched to the time width of the laser pulses used for spectroscopy. Time bunching of the positron pulse is achieved with a fast ramp voltage of ~180 V, applied to the trapping electrodes. This produces pulses containing around 10^5 positrons with a time width of less than 5 ns FWHM, when the system is operated at 1 Hz. The voltage pulse applied to the trap electrodes provides a rough approximation to a harmonic potential[18] except that each trap electrode has its own individually tuned avalanche pulser voltage, which is applied on top of and independently of the DC bias voltage (see Figure 3) and the RF rotating wall voltages for the sections where they are applied. The avalanche voltages have a close to 50 Ω source impedance over a wide range of amplitudes that are obtained from the center tap of a miniature 100 Ω trimmer, the input and output leads of which are connected via 50 Ω resistors to the low output impedance direct avalanche pulser output and to ground. If the total resistance is 4.4×50 Ω (see Figure 6), the output impedance will be within ±10% of 50 Ω as the output is varied from 25% to 75% of full scale. Since the avalanche pulse is coupled capacitively to the output, the bias voltage V_B is directly coupled with a high impedance resistor.

The RF signal for the rotating wall channels is coupled with a 1 kΩ resistor from the high impedance output of a feedback common emitter amplifier and thus is attenuated by only a factor of 2 if $R_L = 1$ kΩ also. This loss of signal is more than compensated by the amplifier gain which is roughly R_L/R_2. In the present circuit all the avalanche transistors are fired by the output of a master avalanche pulser which feeds all of the input transformers via a single turn to each in succession embodied by a single wire from the master output to ground.

The positron pulse width at the location of the target is 3.9 ± 0.1 ns. This was measured using a 3 cm × 3 cm × 2 cm PbF_2 Cherenkov radiator optically coupled to a Hamamatsu R2083 PMT, operated at −1.6 kV. Figure 7 shows the detector response following the impact of the 1 keV positron beam on the metal target holder. The anode signal is recorded at the 50 Ω input of a fast digital oscilloscope (Lecroy HD 04104, with 12 bit vertical resolution, 1 GHz bandwidth, and 2.5 GSa/s sampling rate).

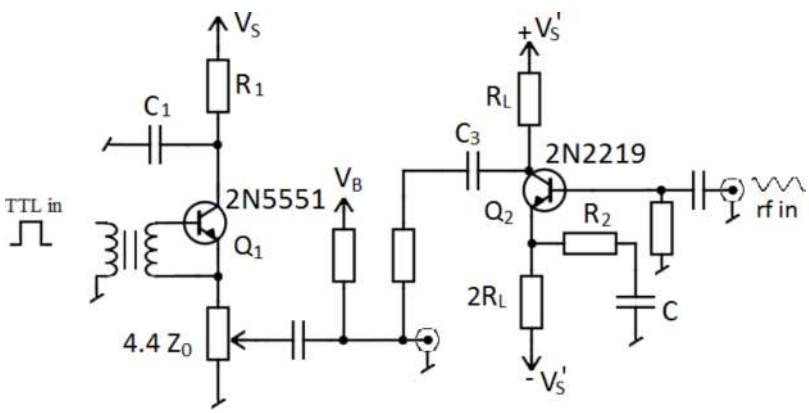

FIG. 6. Circuit diagram showing the avalanche pulser and phase shifter for the rotating wall electrode.[44]

The burst of gamma rays is assumed to have a Gaussian temporal profile, proportional to $\exp(-t^2/2\sigma^2)$. The impulse response of the Cherenkov radiator is an ~100 ps rise associated with the time delay differences from various points in the crystal, followed by an approximately exponential decay with time constant τ due to the multiple light reflections in the radiator during the light collection process.[45] Convolution of a Gaussian function with the variance from the gamma ray burst with the exponential decay of the collected PbF_2 light gives

$$V(t) = \frac{1}{2} A \exp \frac{\sigma^2 - 2t\tau + 2x_0\tau}{2\tau^2} \operatorname{erfc}\left(\frac{-t\tau + x_0\tau + \sigma^2}{\sqrt{2}\sigma\tau}\right), \quad (2)$$

where σ is the Gaussian width, A is the pulse amplitude, x_0 is the centroid of the pulse, and erfc (t) is the complimentary error function. The fitted exponential decay of the light collection time of the radiator is $\tau = 4.0 \pm 0.5$ ns, and we conclude that the gamma ray burst has a FWHM of 3.9 ± 0.1 ns. However, this value will be a slight overestimate as the PMT response time has not been taken into account.

III. POSITRONIUM SPECTROSCOPY

Positronium atoms can be produced by implanting positrons into almost any kind of material.[46–51] For many applications, mesoporous silica films[49,52] are a convenient choice as they can be relatively efficient, require no maintenance, are resilient to radiation and residual gas (at room temperatures), and can be used to generate Ps with different energies simply by changing the incident positron beam energy.[41,53] When a beam of keV positrons is incident on a porous silica target, Ps atoms are formed in the bulk material and then diffuse through an internal pore network, losing energy in the process. For highly interconnected samples, Ps may diffuse back into vacuum with efficiencies of around 20%-30%. In our apparatus, a mesoporous silica target is mounted 8 mm behind a tungsten mesh, which allows us to produce Ps atoms in vacuum in an excitation region with an arbitrary electric field. The geometry of the interaction region is shown in Figure 8.

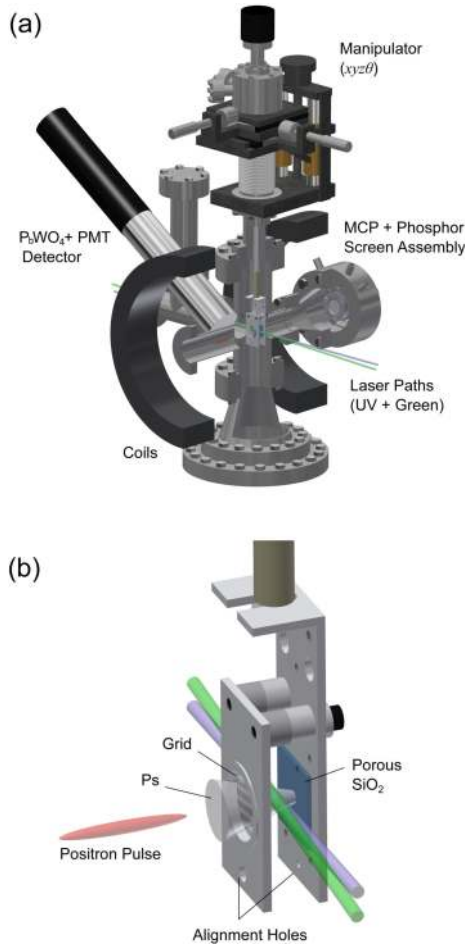

FIG. 8. (a) Positronium-laser interaction chamber. Two coils surround the chamber producing a magnetic field of ~13 mT. The target may be raised out of view of the positron beam for performing trap diagnostics using the MCP. (b) Zoomed SiO_2 porous silica target mount. The target is mounted behind a tungsten grid which is 90% transmissive. Ps atoms are made within the bulk of the material and emitted into vacuum. A 2 mm diameter alignment hole at the bottom of the mount allows calibration of the CCD camera in order to determine the positron beam size at the target. The hole is also used to match the position of the lasers with the emitted Ps.

A. Lasers

The pulsed positron beam system we describe is designed to operate with pulsed lasers that have characteristics typical of Nd:YAG pumped systems. For example, the positron pulses are produced in the few Hz range with a width of around 5 ns, which is well matched to many commercially available laser systems. The other required parameters, such as bandwidth and frequency range, will depend on the experiments to be conducted. We use dye lasers as they are simple to operate and very versatile, but any laser system with short pulses can be used just as easily (for example, optical parametric oscillators[54,55]).

We will describe some of the properties of the lasers we have used to conduct our recent experiments. A pulsed dye laser, operated with coumarin 102 dye, is pumped by the λ = 355 nm third harmonic of a pulsed Nd:YAG laser. This produces light with λ = 486 nm which is frequency doubled by a BBO crystal into a pulse of λ = 243 nm ultraviolet (UV) light. The width of the pulse is ≈6 ns with a $\Delta\nu \approx 85$ GHz bandwidth. The λ = 243 nm light drives single photon 1S-2P atomic transitions in positronium. Following excitation to the 2P state, residual light from the Nd:YAG second harmonic, λ = 532 nm (visible, green), can be used to photoionise the positronium or to pump a second dye laser, in this case operated with styryl-8 dye to produce infrared (IR) light. The fundamental output of this laser gives up to 15 mJ in the range 730-750 nm, which was used to drive 2P-nD transitions in positronium. Both lasers (UV + green or IR) cross paths in front of the SiO_2 target. A schematic of the laser system is shown in Figure 9. In order to synchronise the positron and laser pulses, a plastic scintillator with a pinhole was used to simultaneously observe gamma rays and laser light.[4] The required delay between the positron and laser arrival at the target area will vary depending on the laser position with respect to the target. There is also a dependence on the implantation energy of the positrons, which

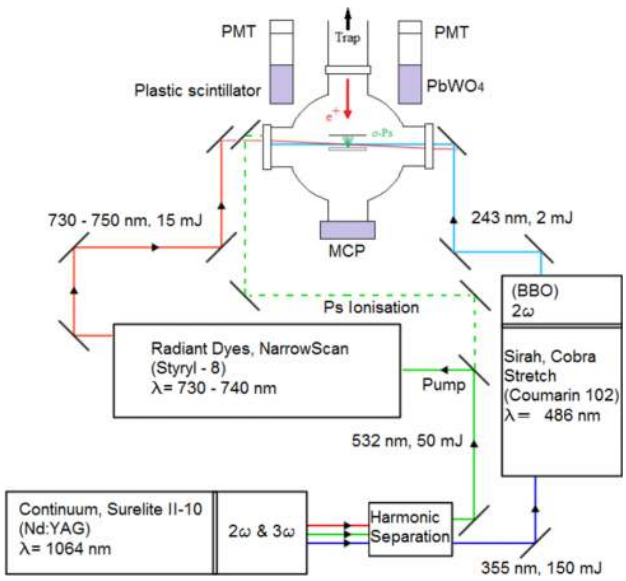

FIG. 9. Laser system schematic. The system can be modified for either 730-750 nm (IR) Rydberg state production or photoionisation of 2P state Ps with residual 532 nm (green) light.

determines both the kinetic energy and the time before the emission of Ps. For 5 keV positrons, the mean emission time is ~10 ns.[56]

B. Single shot positron annihilation lifetime spectroscopy (SSPALS)

The intense positron pulses required to produce a dilute Ps gas mean that conventional gamma ray detection methods cannot be efficiently used. Ordinarily, gamma ray detectors are designed to observe one event at a time. Overlapping events (known as pile up) are usually considered to result in a spurious signal and are rejected.[57] In order to make full use of the information contained in the Ps annihilation radiation, we use a technique called SSPALS.[58] This involves measuring the gamma ray flux with a fast detector and generating a Ps lifetime spectrum, almost in real time. That is, we identify $V(t)$, the PMT anode output, as being proportional to dN/dt, where $N(t)$ is the number of Ps atoms present at time t.

For the majority of our work, we utilise a lead tungstate ($PbWO_4$) scintillator,[45] coupled via a 150 mm long plastic light guide to a PMT (Hamamatsu H10570). The light guide is required only to keep the PMT out of the magnetic field surrounding the target region and has a negligible impact on the time resolution, which is determined mostly by the scintillator decay. $V(t)$ is recorded directly on a fast high-resolution oscilloscope as described in Section II B. $PbWO_4$ is selected for most applications as it has a high gamma ray stopping power (density = 8.3 g/cm^3), a low light output (necessary to avoid saturation of the PMT), and a relatively short scintillation decay time of ~10 ns.[59] Faster detectors are available (see Figure 7) but at the cost of efficiency;[45] in general, detector selection depends on the specific application.

Ps atoms are created predominantly in their ground states,[60] which comprise two spin states, the long-lived S = 1 *ortho*-positronium (*o*-Ps) and the short-lived S = 0 *para*-positronium (*p*-Ps). The lifetimes of these states are 142 ns and 0.125 ns, respectively;[3] this large difference means that any process that converts *o*-Ps into *p*-Ps leads to rapid annihilation, which is relatively easy to observe.

When a positron pulse is implanted into a Ps forming target, fast annihilation events give rise to an initial peak (known as the prompt peak). These are primarily direct positron annihilation and *p*-Ps decay (positron thermalisation and Ps formation processes are typically extremely fast, occurring in a few ps[61]). These events cannot be resolved in our experiments since they occur on a time scale which is much shorter than the incident positron pulse width. Annihilation events that are detected after the prompt peak are due to the decay of long-lived *o*-Ps atoms. Analysing different regions of lifetime spectra to discriminate between these events therefore allows us to determine the amount of *o*-Ps produced and is the basis of the SSPALS methodology.[58] In order to do this, we need only to discriminate between events that occur within the response time of the detector (i.e., within the prompt annihilation peak) and those that occur on the time scale of the *o*-Ps vacuum decay rate (1/142 ns); the ~10 ns decay time of $PbWO_4$ is sufficient for such measurements.

Single shot lifetime spectra are analysed by integrating $V(t)$ over different time regions. From this, we obtain f_d, the fraction of all annihilation events that are delayed with respect to the implantation of the incident positron pulse. When there are no lasers present and Ps atoms are created in vacuum, this fraction is directly related to the amount of Ps produced.[50] If we define the total lifetime spectrum time window as the region A-C and the delayed time window as the region B-C then the delayed fraction (f_d) is given by

$$f_d = \int_B^C V(t)dt \Big/ \int_A^C V(t)dt. \tag{3}$$

As we explain below, the time windows are chosen depending on the process to be studied. We further characterise laser induced changes in the Ps decay rates using the parameter S, which is given by

$$S = \frac{f_{\mathrm{bk}} - f_{\mathrm{sig}}}{f_{\mathrm{bk}}}, \tag{4}$$

where f_{sig} and f_{bk} refer to signal and background measurements of f_d, respectively. Exactly what constitutes a signal and background measurement will depend on what is being measured. In the most simple case, it could refer to measurements taken with (f_{sig}) and without (f_{bk}) a laser pulse. However, it could also refer to a more complicated arrangement in which the background was actually the production of 2P states, and the signal was the excitation of these states to Rydberg levels. In this case f_{bk} would be recorded with a resonant UV (243 nm) laser, f_{sig} with an IR and a UV laser, and S would then be a measure of the number of 2P atoms excited into Rydberg states.

There are three principal types of experiments in which optically excited Ps atoms are studied using SSPALS, these are: (1) the excitation of Ps into short-lived states, (2) Ps excitation into long-lived states, and (3) Ps excitation at variable times. These experiments all require slightly different forms of analysis. We define long and short-lived with respect to the

142 ns ground state lifetime, although for some measurements the ground state Ps lifetime may be modified, for example, if it is confined in a porous medium.[22]

1. Excitation to short-lived states

Because Ps atoms emitted from most targets are somewhat divergent and fast, it is generally necessary to excite them as soon as possible after they have been created (that is, immediately after the incident positron pulse). When atoms are optically excited to the 2P state, several processes can occur. They can simply decay radiatively back to the *o*-Ps ground state, they can be photoionised or, if there is a magnetic field present, they can undergo a process known as magnetic quenching in which Zeeman mixed states provide a route to radiatively decay to the *p*-Ps ground state.[62,63] Atoms that end up back in their long-lived ground state (either due to spontaneous or stimulated decay) produce no observable effect; at most this will result in a factor of two reduction in the Ps decay rate, but only for the duration of the laser pulse. Photoionisation generally results in the liberated positron colliding with the target at low energy and annihilating. Similarly, magnetic quenching results in fast annihilation since the *p*-Ps lifetime is short.[3]

Rapid annihilation events of this type will change the single-shot lifetime spectra by increasing the number of decay photons appearing at early times, with a corresponding decrease in the decays at later times. To analyse such processes, the time window is set as close to the prompt peak as possible. An example is shown in Figure 10. The top panel (a) shows SSPALS spectra taken with a 1S-2P excitation laser both on and off resonance, as well as a 532 nm photoionisation laser. Here, the time windows used are $A = -3$ ns, $B = 35$ ns, and $C = 350$ ns. A is negative since we define t_0 relative to the rising edge of the prompt peak, as determined by a constant fraction discrimination algorithm. Panel (b) shows the difference between the laser on and off data. The excess counts at early times and the deficit at later times are clearly visible. The reduction in the long-lived laser on signal is also visible in the lifetime spectra. Since f_d decreases when the laser is fired (and Ps annihilation is induced), the S value derived here will be positive. This is seen in Figure 10(c), which shows S measured for different wavelengths. $S(\lambda)$ constitutes a measurement of the Doppler-broadened 1S-2P line shape.

For measurements of this type, the time reference B is selected as the cross-over point between positive and negative signals in the difference signal. This is done to optimise the laser induced signal. The value of C is less important and is normally selected to exclude the later, noisier part of the spectrum. The line shape for the transition has been fitted with the Gaussian function,

$$S(\lambda) = A \exp \frac{-(\lambda - \lambda_0)^2}{(2\sigma^2)}, \tag{5}$$

where the Gaussian width (σ) and the resonant wavelength ($\lambda_0 = 243$ nm) are related to the RMS velocity of the emitted positronium in the direction parallel to the laser by $v_{\mathrm{RMS}\|} = c\frac{\sigma}{\lambda_0}$. In this particular case, we measure $v_{\mathrm{RMS}\|} = 9.6 \pm 0.2 \times 10^4$ m/s, which is typical for Ps atoms emitted from porous silica films.[53]

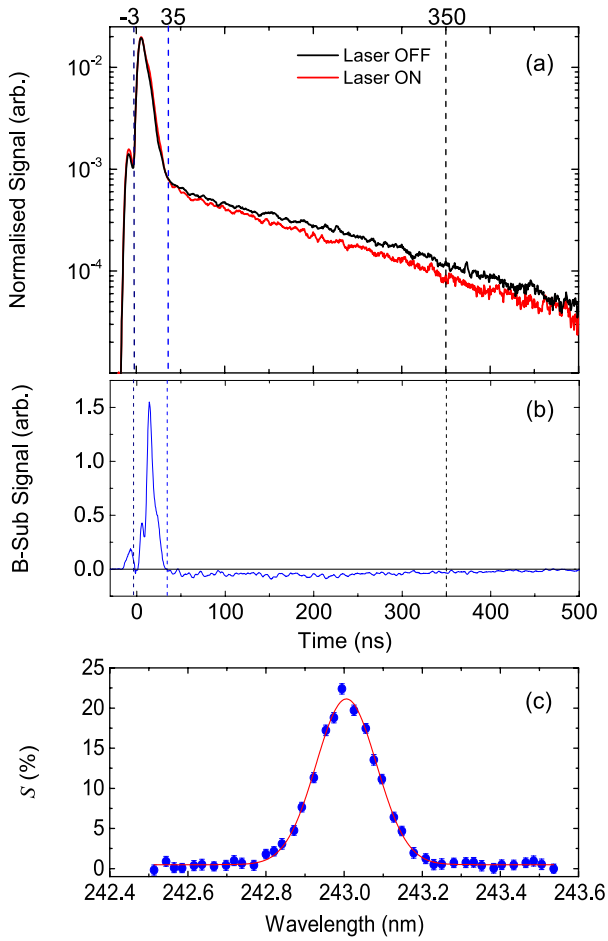

FIG. 10. (a) SSPALS spectra comparing data with the laser on and off resonance with the 1S-2P transition in Ps; the data are normalised to have the same total area. The 1S-2P excitation was driven with UV light (2 mJ). 2P states are photoionised with 532 nm pulses (20 mJ). The small bump at the very early part of the spectrum is due to some positrons annihilating on a pumping restriction before they arrive at the interaction region. (b) The difference between the two lifetime spectra shown in (a). The vertical lines indicate the time windows used to analyse these data, namely, A = −3 ns, B = 35 ns, and C = 350 ns. (c) The Doppler broadened 1S-2P line shape measured using this methodology. The solid line is a fitted Gaussian function with a width of 0.18 ± 0.03 nm FWHM. This represents Ps with an effective temperature of 580 ± 15 K.

2. Excitation to long-lived states

The analysis used for short-lived Ps states as described above is not well suited for cases where long-lived states are produced. That is, if Rydberg atoms are generated that may live for times that are long compared to 142 ns, different time windows should be used for the analysis. In some cases it may not be possible to use SSPALS techniques at all, for example, if the Ps atoms move far away from the detector in their lifetime. The generation of long lived states could, however, be detected if these states are subsequently ionised at a later time or if their lifetimes are of the order of a few hundred ns. An example of such an experiment is shown in Figure 11. In this case, Rydberg Ps atoms were generated with principal quantum number

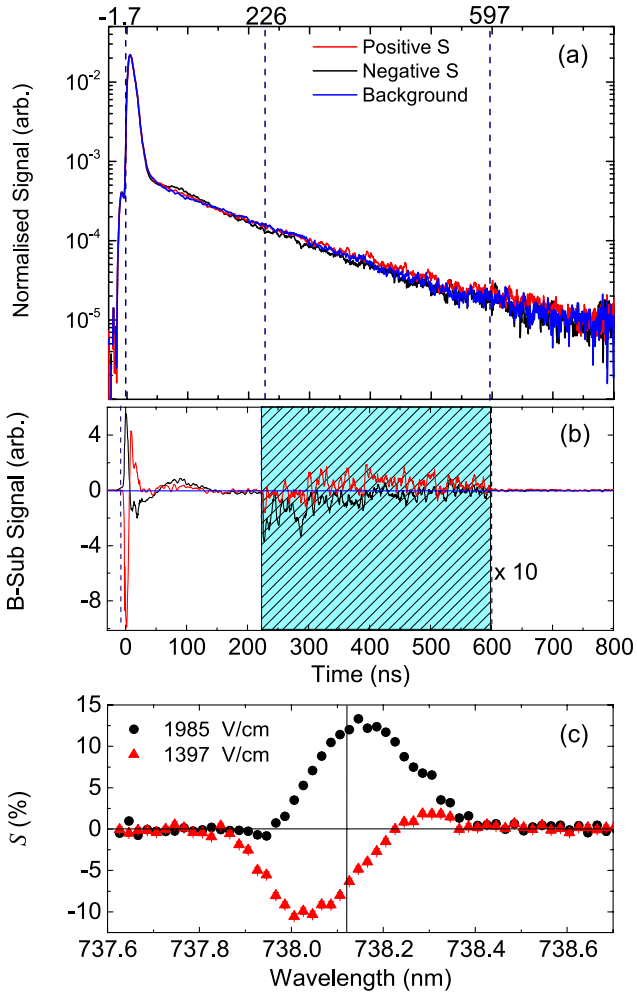

FIG. 11. (a) Area-normalised SSPALS spectra comparing the detection of transmitted and field ionised $n = 18$ Ps atoms with positive and negative Stark shifts, respectively. The background spectrum obtained with the UV laser on resonance but the IR laser off resonance is also shown. (b) Difference spectra obtained using the data shown in (a). The data in the shaded region in (b) between the windows *B*-*C* have been multiplied by 10 for clarity. (c) Measured S values as a function of IR wavelength for two electric fields outside the grid region of 1397 V/cm and 1985 V/cm, which allow and prevent transmission of almost all Ps through the grid. These data are discussed in detail elsewhere.[23] The vertical line in (c) denotes the position of the field free $n = 18$ wavelength. The size of the error bars is comparable to the point size.

$n = 18$ using a two step ($1S \rightarrow 2P \rightarrow nD/nS$) optical transition.[23] These states can live for hundreds of ns (due to state mixing and collisions with the chamber walls) and so, appropriate time windows are selected for these experiments, as indicated in the figure.

An interesting aspect of this measurement is that the Rydberg Ps atoms pass through a grid (see Figure 8). Depending on the electric field near the grid, Ps atoms can be forced to annihilate there or they can be allowed to continue travelling forward. Since the grid is 0.8 cm from the Ps formation target, the flight time is of the order of 100 ns. Thus, with the time windows shown in Figure 11, annihilation on the grid will result in a positive S value, whereas annihilations later than 226 ns will give rise to a negative S signal. This is indeed what is observed, as shown in Figure 11(c). The negative S values represent atoms that are transmitted through the grid and are not detected within the window *B*-*C*. If *B* is set to 35 ns, as in the previous example, no Rydberg Ps atoms are detected.

3. Excitation in variable time windows

SSPALS can also be used to perform optical measurements with Ps atoms that are excited and photoionised at variable times after the prompt peak. For experiments of this type, the appropriate integration regions will depend on when the laser is fired, and hence, the analysis will be performed using a variable time window. This idea has been used to perform laser-enhanced positronium time-of-flight (LEPTOF) measurements.[56] In this work, the laser delay time and position relative to the target are varied, making it possible to measure the Ps time-of-flight distribution in the direction perpendicular to the target surface. An example of such a measurement is shown in Figure 12. When the laser is fired at different times, an excess of gamma rays is detected, visible as the peaks in Figures 12(a) and 12(b). The amount of excess annihilation radiation observed is related to the number of atoms present at the location and time of the laser pulse. Changes in the

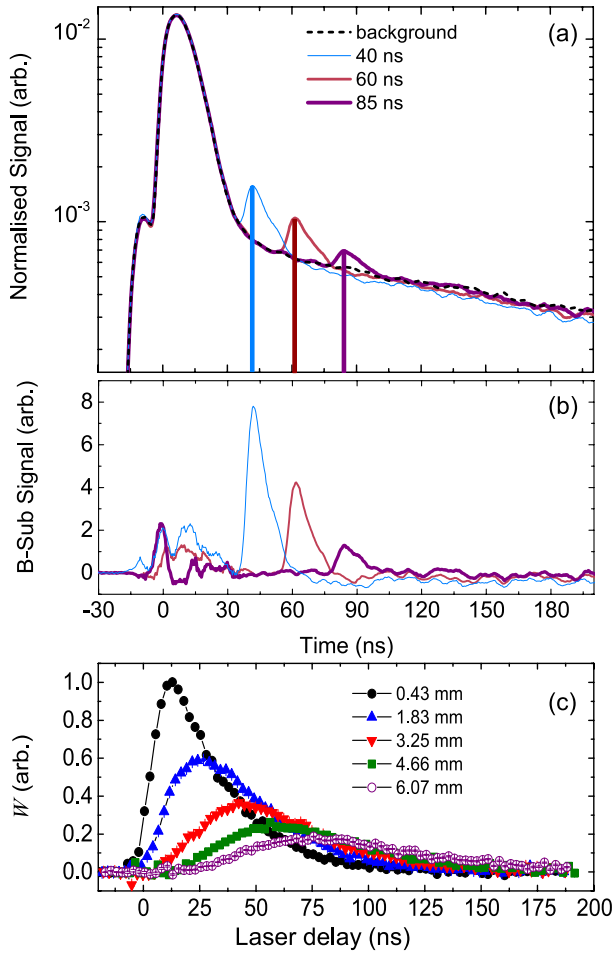

FIG. 12. (a) Area-normalised SSPALS spectra showing the excess annihilations observed when firing the lasers at different times relative to the positron pulse. Each waveform is the average of 120 shots. The shaded regions represent the laser interaction window, which is 4 ns wide and centred about the laser arrival time. (b) Difference spectra of the data in (a). (c) Background-subtracted and decay-corrected time-of-flight distributions plotted for varying distances between the target and the laser. The size of the error bars is comparable to the point size.

annihilation spectra are quantified in this case by the quantity W, which is the mean value of a background-subtracted and decay-corrected spectrum evaluated during a 4 ns integration window centred at the arrival of the laser. W is given by

$$W = \frac{1}{\tau}\int_{t_1}^{t_2}[V(t)_{\text{on}} - V(t)_{\text{off}}]\exp^{t/142}dt, \qquad (6)$$

where τ is the length of the integration window (t_2-t_1), which in this case is 4 ns. The subscripts on and off refer to the UV wavelength, which is tuned on and off resonance with the 1S-2P transition (243.01 and 242.25 nm, respectively) for background subtraction. The exponential term takes into account the decay of Ps atoms in the time between their creation and the laser excitation. As in the case of short lived state production (Figure 10), the difference spectra (Figure 12(b)) reveal the laser induced changes directly.

In order to conduct LEPTOF measurements, the position of the laser beam must be well defined relative to the target surface. Then, $W(t)$ gives the arrival time of a distribution of Ps atoms at a point in space, from which we generate a time-of-flight distribution, as shown in Figure 12(c). These data show the emission and flight time of Ps atoms produced in the bulk of a porous SiO_2 silica sample.[56] This methodology has many advantages over conventional Ps TOF measurements.[64] For example, it is ordinarily necessary to observe the annihilation of atoms through a narrow aperture to define the spatial region. This means that only those atoms that happen to decay in the field of view of the detector will be observed, whereas in LEPTOF measurements, the laser beams produce a well-defined volume for annihilation, dramatically increasing the detection efficiency and spatial resolution. However, it is extremely important to properly account for the velocity dependence of the excitation and ionisation processes, and in general, LEPTOF spectroscopy is best suited to studying very low energy Ps atoms.

IV. APPLICATIONS

An example of recent work that has been performed using the methods described above is the production of Rydberg states of positronium. This is part of an experimental programme that has long term goals in the manipulation and deceleration of these atoms via interactions with their large dipole moments.[23,65,66] A spectrum of transitions from n = 2 to Ps Rydberg states with principal quantum numbers n in the range 11-22 is shown in Figure 13.

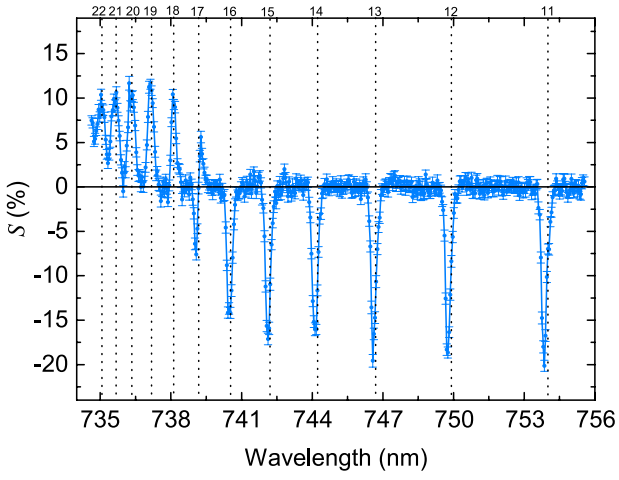

FIG. 13. Population of high n states in positronium. These data were collected with a small electric field between the target and grid (~63 V/cm). The dashed lines indicate the expected resonant wavelengths in accordance with the Rydberg formula.

These states were prepared in a small electric field of ~63 V/cm using the two-step 1S → 2P → nD/nS excitation scheme described in Sec. III.

The field ionisation of atoms which travel through a grid (see Figure 8) with n greater than 17 results in the inversion of the parameter S. The fact that some of the n = 17 states exhibit positive S and some negative is due to the fact that different Stark states are ionised in different electric fields, which means that the timing signal allows some discrimination

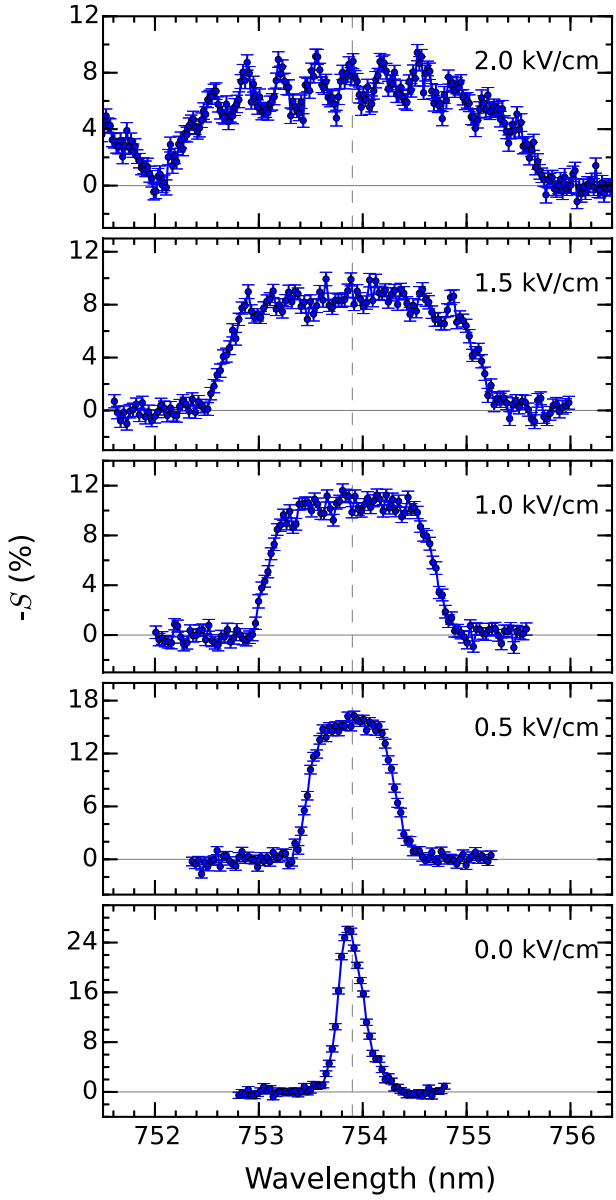

FIG. 14. Stark broadening of n = 11 Ps states in various electric fields, as indicated in the panels. The dashed line represents the expected IR transition wavelength at zero field. For the highest field (2 kV/cm), the encroachment of neighbouring n = 12 states can be seen at the shorter wavelengths. The individual Stark states can be partially resolved at the highest field, but are limited by the 85 GHz bandwidth of the 1S-2P excitation laser.

between Stark states, even though they cannot be spectrally resolved.

By increasing the electric field in the laser interaction region, Rydberg Ps states become Stark broadened, as shown in Figure 14 for $n = 11$. These data show S values as a function of IR wavelength for varying electric fields. For 2000 V/cm, individual Stark states can be partially resolved with a spectral resolution of 85 GHz. A flat electric field was produced by creating a potential difference between the target and the grid (Figure 8). As the electric field is increased, individual Stark states with equal values of the azimuthal quantum number $|m_\ell|$ are separated in frequency. For these measurements, the time windows used are the same as those in Figure 11 ($A = -1.7$ ns, $B = 226$ ns, and $C = 597$ ns).

V. SUMMARY

The techniques described above make it possible to perform a number of experiments in which Ps atoms are optically excited. Our apparatus can produce positron pulses with areal densities of around 10^6 cm^{-2}, leading to an initial Ps density of around 10^{11} cm^{-3} for Ps confined in a porous film (although there may well be an effective density enhancement in this case[22]). For Ps in vacuum, the achievable densities are of the order of 10^7 cm^{-3}, although this will decrease rapidly as atoms move away from the surface. These densities are comparable to, for example, the densities of atomic beams used for laser cooling experiments.[67]

The production of a dilute Ps gas from a pulsed positron beam is complemented by using single shot detection methods described in Section III B. Together these methods allow Ps to be efficiently utilised, which is advantageous given the relatively low numbers of atoms available. This point is illustrated by considering the first experiments in which Rydberg Ps was produced.[5] In that work, an intense pulsed positron beam was used[9] that was capable of providing more than an order of magnitude more positrons than the system we describe here. However, the ability to observe excited Ps states was limited by the single-event detection scheme,[63] and as a result, we are able to generate data with vastly improved statistics using fewer positrons.

The system we have described is optimised for laser interrogation of Ps atoms. The versatility of the SSPALS detection methodology allows for a wide variety of experiments such as the characterisation of Ps forming materials, fundamental studies of Ps atoms (including Ps spectroscopy), and the generation and manipulation of long-lived Rydberg states. In future work, we expect to be able to perform precise measurements using more sophisticated laser systems. For example, a transform limited laser derived from a diode seeded pulsed dye amplifier would have a bandwidth of a few hundred MHz and would enable spectroscopic measurements as well as direct Doppler-free two-photon excitation to Rydberg states.[68]

ACKNOWLEDGMENTS

The authors are grateful to R. Jawad and J. Dumper for technical assistance and to L. Liszkay for providing silica samples. We are also grateful to A. P. Mills, Jr., for useful discussions and for designing and building the pulser electronics. This work was supported by UCL through its Impact Studentship Programme and was funded in part by the Leverhulme trust (Grant No. RPG-2013-055), the European Research Council (Grant No. CIG 630119), and the UK Engineering and Physical Sciences Research Council (Grant No. EP/K028774/1).

[1]K. F. Canter, P. G. Coleman, T. C. Griffith, and G. R. Heyland, "Measurement of total cross sections for low energy positron-helium collisions (positron backscattering from metal surface)," J. Phys. B: At. Mol. Phys. **5**, L167 (1972).
[2]M. Charlton and J. W. Humberston, *Positron Physics* (Cambridge University Press, Cambridge, New York, England, 2001).
[3]A. Rich, "Recent experimental advances in positronium research," Rev. Mod. Phys. **53**, 127–165 (1981).
[4]S. Chu and A. P. Mills, Jr., "Excitation of the positronium $1^3S_1 \rightarrow 2^3S_1$ two-photon transition," Phys. Rev. Lett. **48**, 1333–1337 (1982).
[5]K. P. Ziock, R. H. Howell, F. Magnotta, R. A. Failor, and K. M. Jones, "First observation of resonant excitation of high-n states in positronium," Phys. Rev. Lett. **64**, 2366–2369 (1990).
[6]M. S. Fee, A. P. Mills, Jr., S. Chu, E. D. Shaw, K. Danzmann, R. J. Chichester, and D. M. Zuckerman, "Measurement of the positronium $1^3S_1 - 2^3S_1$ interval by continuous-wave two-photon excitation," Phys. Rev. Lett. **70**, 1397–1400 (1993).
[7]S. Chu, A. P. Mills, Jr., and J. L. Hall, "Measurement of the positronium $1^3S_1 - 2^3S_1$ interval by Doppler-free two-photon spectroscopy," Phys. Rev. Lett. **52**, 1689–1692 (1984).
[8]A. P. Mills, Jr., E. D. Shaw, R. J. Chichester, and D. M. Zuckerman, "Production of slow positron bunches using a microtron accelerator," Rev. Sci. Instrum. **60**, 825–830 (1989).
[9]R. Howell, M. Fluss, I. Rosenberg, and P. Meyer, "Low-energy, high-intensity positron beam experiments with a linac," Nucl. Instrum. Methods Phys. Res., Sect. B **10–11**(Part 1), 373–377 (1985).
[10]K. Michishio, T. Tachibana, H. Terabe, A. Igarashi, K. Wada, T. Kuga, A. Yagishita, T. Hyodo, and Y. Nagashima, "Photodetachment of positronium negative ions," Phys. Rev. Lett. **106**, 153401 (2011).
[11]Y. Nagashima, "Experiments on positronium negative ions," Phys. Rep. **545**, 95–123 (2014).
[12]C. M. Surko, M. Leventhal, and A. Passner, "Positron plasma in the laboratory," Phys. Rev. Lett. **62**, 901–904 (1989).
[13]J. R. Danielson, D. H. E. Dubin, R. G. Greaves, and C. M. Surko, "Plasma and trap-based techniques for science with positrons," Rev. Mod. Phys. **87**, 247–306 (2015).
[14]M. R. Natisin, J. R. Danielson, and C. M. Surko, "Formation of buffer-gas-trap based positron beams," Phys. Plasmas **22**, 033501 (2015).
[15]J. P. Marler and C. M. Surko, "Positron-impact ionization, positronium formation, and electronic excitation cross sections for diatomic molecules," Phys. Rev. A **72**, 062713 (2005).
[16]G. F. Gribakin, J. A. Young, and C. M. Surko, "Positron-molecule interactions: Resonant attachment, annihilation, and bound states," Rev. Mod. Phys. **82**, 2557–2607 (2010).
[17]A. C. L. Jones, P. Caradonna, C. Makochekanwa, D. S. Slaughter, R. P. McEachran, J. R. Machacek, J. P. Sullivan, and S. J. Buckman, "Observation of threshold effects in positron scattering from the noble gases," Phys. Rev. Lett. **105**, 073201 (2010).
[18]A. P. Mills, Jr., "Time bunching of slow positrons for annihilation lifetime and pulsed laser photon absorption experiments," Appl. Phys. **22**, 273–276 (1980).
[19]J. P. Sullivan, J. Roberts, R. W. Weed, M. R. Went, D. S. Newman, and S. J. Buckman, "A trap-based positron beamline for the study of materials," Meas. Sci. Technol. **21**, 085702 (2010).
[20]R. G. Greaves and J. Moxom, "Design and performance of a trap based positron beam source," AIP Conf. Proc. **692**, 140 (2003).
[21]D. B. Cassidy, S. H. M. Deng, R. G. Greaves, and A. P. Mills, Jr., "Accumulator for the production of intense positron pulses," Rev. Sci. Instrum. **77**, 073106 (2006).
[22]D. B. Cassidy and A. P. Mills, Jr., "Enhanced Ps-Ps interactions due to quantum confinement," Phys. Rev. Lett. **107**, 213401 (2011).
[23]T. E. Wall, A. M. Alonso, B. S. Cooper, A. Deller, S. D. Hogan, and D. B. Cassidy, "Selective production of Rydberg-Stark states of positronium," Phys. Rev. Lett. **114**, 173001 (2015).

[24]J. P. Sullivan, S. J. Gilbert, J. P. Marler, R. G. Greaves, S. J. Buckman, and C. M. Surko, "Positron scattering from atoms and molecules using a magnetized beam," Phys. Rev. A **66**, 042708 (2002).
[25]J. Clarke, D. P. van der Werf, B. Griffiths, D. C. S. Beddows, M. Charlton, H. H. Telle, and P. R. Watkeys, "Design and operation of a two-stage positron accumulator," Rev. Sci. Instrum. **77**, 063302 (2006).
[26]J. P. Sullivan, A. Jones, P. Caradonna, C. Makochekanwa, and S. J. Buckman, "A positron trap and beam apparatus for atomic and molecular scattering experiments," Rev. Sci. Instrum. **79**, 113105 (2008).
[27]S. Andersen, R. Johansen, J. Overgaard, J. Mortensen, K. Andersen, H. Thomsen, M. Lund, J. Chevallier, H. Knudsen, and U. Uggerhøj, "Positronium formation from porous silica in backscattering and transmission geometries," Eur. Phys. J. D **68**, 124 (2014).
[28]T. R. Weber, J. R. Danielson, and C. M. Surko, "Note: Electrostatic beams from a 5 T Penning—Malmberg trap," Rev. Sci. Instrum. **82**, 016104 (2011).
[29]D. Comeau, A. Dror, D. W. Fitzakerley, M. C. George, E. A. Hessels, C. H. Storry, M. Weel, D. Grzonka, W. Oelert, G. Gabrielse, R. Kalra, W. S. Kolthammer, R. McConnell, P. Richerme, A. Müllers, J. Walz, and ATRAP Collaboration, "Efficient transfer of positrons from a buffer-gas-cooled accumulator into an orthogonally oriented superconducting solenoid for antihydrogen studies," New J. Phys. **14**, 045006 (2012).
[30]C. Amole, G. Andresen, M. Ashkezari, M. Baquero-Ruiz, W. Bertsche, P. Bowe, E. Butler, A. Capra, P. Carpenter, C. Cesar, S. Chapman, M. Charlton, A. Deller, S. Eriksson, J. Escallier, J. Fajans, T. Friesen, M. Fujiwara, D. Gill, A. Gutierrez, J. Hangst, W. Hardy, R. Hayano, M. Hayden, A. Humphries, J. Hurt, R. Hydomako, C. Isaac, M. Jenkins, S. Jonsell, L. Jørgensen, S. Kerrigan, L. Kurchaninov, N. Madsen, A. Marone, J. McKenna, S. Menary, P. Nolan, K. Olchanski, A. Olin, B. Parker, A. Povilus, P. Pusa, F. Robicheaux, E. Sarid, D. Seddon, S. S. E. Nasr, D. Silveira, C. So, J. Storey, R. Thompson, J. Thornhill, D. Wells, D. van der Werf, J. Wurtele, and Y. Yamazaki, "The ALPHA antihydrogen trapping apparatus," Nucl. Instrum. Methods Phys. Res., Sect. A **735**, 319–340 (2014).
[31]*Positron Beams and Their Applications*, edited by P. Coleman (World Scientific, Singapore, 2000).
[32]P. J. Schultz and K. G. Lynn, "Interaction of positron beams with surfaces, thin films, and interfaces," Rev. Mod. Phys. **60**, 701–779 (1988).
[33]A. P. Mills, Jr. and E. M. Gullikson, "Solid neon moderator for producing slow positrons," Appl. Phys. Lett. **49**, 1121 (1986).
[34]M. R. Khatri, M. Charlton, P. Sferiazzo, K. G. Lynn, A. P. Mills, Jr., and L. O. Roellig, "Improvement of rare-gas solid moderators by using conical geometry," Appl. Phys. Lett. **57**, 2374 (1990).
[35]T. J. Murphy and C. M. Surko, "Positron trapping in an electrostatic well by inelastic collisions with nitrogen molecules," Phys. Rev. A **46**, 5696–5705 (1992).
[36]M. R. Natisin, J. R. Danielson, and C. M. Surko, "Positron cooling by vibrational and rotational excitation of molecular gases," J. Phys. B: At., Mol. Opt. Phys. **47**, 225209 (2014).
[37]R. G. Greaves and J. M. Moxom, "Compression of trapped positrons in a single particle regime by a rotating electric field," Phys. Plasmas **15**, 072304 (2008).
[38]C. A. Isaac, C. J. Baker, T. Mortensen, D. P. van der Werf, and M. Charlton, "Compression of positron clouds in the independent particle regime," Phys. Rev. Lett. **107**, 033201 (2011).
[39]A. P. Mills, Jr., "Brightness enhancement of slow positron beams," Appl. Phys. **23**, 189–191 (1980).
[40]A. Deller, T. Mortensen, C. A. Isaac, D. P. van der Werf, and M. Charlton, "Radially selective inward transport of positrons in a Penning–Malmberg trap," New J. Phys. **16**, 073028 (2014).
[41]D. B. Cassidy, P. Crivelli, T. H. Hisakado, L. Liszkay, V. E. Meligne, P. Perez, H. W. K. Tom, and A. P. Mills, Jr., "Positronium cooling in porous silica measured via Doppler spectroscopy," Phys. Rev. A **81**, 012715 (2010).
[42]D. B. Cassidy and A. P. Mills, Jr., "Interactions between positronium atoms in porous silica," Phys. Rev. Lett. **100**, 013401 (2008).
[43]D. B. Cassidy, T. H. Hisakado, H. W. K. Tom, and A. P. Mills, Jr., "Optical spectroscopy of molecular positronium," Phys. Rev. Lett. **108**, 133402 (2012).
[44]A. P. Mills, Jr., private communication (2014).
[45]D. B. Cassidy and A. P. Mills, Jr., "A fast detector for single-shot positron annihilation lifetime spectroscopy," Nucl. Instrum. Methods Phys. Res., Sect. A **580**, 1338–1343 (2007).
[46]K. F. Canter, A. P. Mills, Jr., and S. Berko, "Efficient positronium formation by slow positrons incident on solid targets," Phys. Rev. Lett. **33**, 7–10 (1974).
[47]A. P. Mills, Jr., "Positronium formation at surfaces," Phys. Rev. Lett. **41**, 1828–1831 (1978).
[48]Y. Nagashima, Y. Morinaka, T. Kurihara, Y. Nagai, T. Hyodo, T. Shidara, and K. Nakahara, "Origins of positronium emitted from SiO_2," Phys. Rev. B **58**, 12676–12679 (1998).
[49]L. Liszkay, C. Corbel, P. Perez, P. Desgardin, M.-F. Barthe, T. Ohdaira, R. Suzuki, P. Crivelli, U. Gendotti, A. Rubbia, M. Etienne, and A. Walcarius, "Positronium reemission yield from mesostructured silica films," Appl. Phys. Lett. **92**, 063114 (2008).
[50]D. B. Cassidy, T. H. Hisakado, H. W. K. Tom, and A. P. Mills, Jr., "Positronium formation via excitonlike states on Si and Ge surfaces," Phys. Rev. B **84**, 195312 (2011).
[51]A. C. L. Jones, H. J. Goldman, Q. Zhai, P. Feng, H. W. K. Tom, and A. P. Mills, Jr., "Monoenergetic positronium emission from metal-organic framework crystals," Phys. Rev. Lett. **114**, 153201 (2015).
[52]L. Liszkay, F. Guillemot, C. Corbel, J.-P. Boilot, T. Gacoin, E. Barthel, P. Pérez, M.-F. Barthe, P. Desgardin, P. Crivelli, U. Gendotti, and A. Rubbia, "Positron annihilation in latex-templated macroporous silica films: Pore size and ortho-positronium escape," New J. Phys. **14**, 065009 (2012).
[53]P. Crivelli, U. Gendotti, A. Rubbia, L. Liszkay, P. Perez, and C. Corbel, "Measurement of the orthopositronium confinement energy in mesoporous thin films," Phys. Rev. A **81**, 052703 (2010).
[54]M. Becucci, G. Ferrari, I. Boscolo, F. Castelli, S. Cialdi, F. Villa, and M. Giammarchi, "Laser sources for efficient two-step positronium excitation to Rydberg states," in *Molecular Spectroscopy and Molecular Structure, A Collection of Papers Presented at the XXXth European Congress on Molecular Spectroscopy, Florence, Italy, August 29–September 3* (2010) [J. Mol. Struct. **993**, 495–499 (2011)].
[55]A. Deller, D. Edwards, T. Mortensen, C. A. Isaac, D. P. van der Werf, H. H. Telle, and M. Charlton, "Exciting positronium with a solid-state UV laser: The Doppler-broadened Lyman-α transition," J. Phys. B: At. Mol. Phys. **48**, 175001 (2015).
[56]A. Deller, B. S. Cooper, T. E. Wall, and D. B. Cassidy, "Positronium emission from mesoporous silica studied by laser-enhanced time-of-flight spectroscopy," New J. Phys. **17**, 043059 (2015).
[57]G. F. Knoll, *Radiation Detection and Measurement*, 4th ed. (John Wiley & Sons, 2010).
[58]D. B. Cassidy, S. H. M. Deng, H. K. M. Tanaka, and A. P. Mills, Jr., "Single shot positron annihilation lifetime spectroscopy," Appl. Phys. Lett. **88**, 194105 (2006).
[59]A. Annenkov, M. Korzhik, and P. Lecoq, "Lead tungstate scintillation material," Nucl. Instrum. Methods Phys. Res., Sect. A **490**, 30–50 (2002).
[60]K. F. Canter, A. P. Mills, Jr., and S. Berko, "Observations of positronium Lyman-α radiation," Phys. Rev. Lett. **34**, 177–180 (1975).
[61]R. M. Nieminen and J. Oliva, "Theory of positronium formation and positron emission at metal surfaces," Phys. Rev. B **22**, 2226–2247 (1980).
[62]S. M. Curry, "Combined Zeeman and motional effects in the first excited state of positronium," Phys. Rev. A **7**, 447–450 (1973).
[63]K. P. Ziock, C. D. Dermer, R. H. Howell, F. Magnotta, and K. M. Jones, "Optical saturation of the 1^3s-2^3p transition in positronium," J. Phys. B: At., Mol. Opt. Phys. **23**, 329 (1990).
[64]A. P. Mills, Jr. and L. Pfeiffer, "Desorption of surface positrons: A source of free positronium at thermal velocities," Phys. Rev. Lett. **43**, 1961–1964 (1979).
[65]D. B. Cassidy and S. D. Hogan, "Atom control and gravity measurements using Rydberg positronium," Int. J. Mod. Phys.: Conf. Ser. **30**, 1460259 (2014).
[66]S. D. Hogan, P. Allmendinger, H. Saßmannshausen, H. Schmutz, and F. Merkt, "Surface-electrode Rydberg-Stark decelerator," Phys. Rev. Lett. **108**, 063008 (2012).
[67]S. Chu, L. Hollberg, J. E. Bjorkholm, A. Cable, and A. Ashkin, "Three-dimensional viscous confinement and cooling of atoms by resonance radiation pressure," Phys. Rev. Lett. **55**, 48–51 (1985).
[68]T. E. Wall, D. B. Cassidy, and S. D. Hogan, "Single-color two-photon spectroscopy of Rydberg states in electric fields," Phys. Rev. A **90**, 053430 (2014).